Differential cross section polarization moments: Location of the D-atom transfer in the transition-state region for the reactions $Cl+C_2D_6 \rightarrow DCl(v'=0,J'=1)+C_2D_5$ and $Cl+CD_4 \rightarrow DCl(v'=0,J'=1)+CD_3$

T. Peter Rakitzis, S. Alex Kandel, Topaz Lev-On, and Richard N. Zare
Department of Chemistry, Stanford University, Stanford, California 94305

(Received 7 July 1997; accepted 2 September 1997)

The photoloc technique can permit the measurement of not only the state-to-state differential cross section but also its complete product polarization dependence for all moments of orientation and alignment with $k \leqslant 2$. We have realized this possibility for the reaction $Cl+C_2D_6 \rightarrow DCl(v'=0,J'=1)+C_2D_5$ at a collision energy of 0.25 eV, for which we have measured the differential cross section, $1/\sigma(d\sigma_{00}/d\Omega_r)$, and the four polarization-dependent moments of the differential cross section, $A_1^{(1)\mathrm{stf}}$, $A_0^{(2)\mathrm{stf}}$, $A_1^{(2)\mathrm{stf}}$, and $A_2^{(2)\mathrm{stf}}$, in the stationary target frame (STF), which are defined by $A_q^{(k)\mathrm{stf}}=(d\sigma_{kq}^{\mathrm{stf}}/d\Omega_r)/(d\sigma_{00}/d\Omega_r)$. For the $Cl+CD_4 \rightarrow DCl(v'=0,J'=1)+CD_3$ reaction at a collision energy of 0.28 eV we have also determined $1/\sigma(d\sigma_{00}/d\Omega_r)$ and $A_0^{(2)\mathrm{stf}}$. The laboratory speed distributions of the $DCl(v'=0,J'=1)$ products are measured using $2+1$ resonance-enhanced multiphoton ionization (REMPI) and the core-extraction technique. The polarization-dependent differential cross sections are determined from the dependence of the core-extracted profiles on the photolysis and probe polarizations. Recent studies have shown that the $Cl+CD_4$ and $Cl+C_2D_6$ both show scattering behavior described by the line-of-centers model and both yield rotationally cold DCl products with little energy in the alkyl fragments. Despite these similarities, we measure $DCl(v'=0,J'=1)$ product polarizations that differ greatly for these two reactions. For the $Cl+CD_4$ reaction, we find that J_{DCl} is maximally aligned perpendicular to an axis close to the product scattering direction, u_{DCl}. For the $Cl+C_2D_6$ reaction, we find that J_{DCl} is half-maximally aligned perpendicular to the line-of-centers direction. We interpret these results in terms of the location of the D-atom transfer along the reaction coordinate, positing that the D-atom transfer for the $Cl+CD_4$ reaction occurs late in the reactive process and the D-atom transfer for the $Cl+C_2D_6$ reaction occurs earlier near the distance of closest approach. We interpret the difference in the locations of the D-atom transfer to be the cause of the large differences in the Arrhenius pre-exponential factors of the $Cl+CD_4$ and $Cl+C_2D_6$ reactions. © *1997 American Institute of Physics.*
[S0021-9606(97)00346-2]

I. INTRODUCTION

In recent decades, experimental and theoretical efforts to elucidate the dynamics of bimolecular reactions have focused on the state-to-state reactive scattering process. There has been considerable success in connecting the scattering dynamics to a reactive mechanism or to features of the potential-energy surface.[1] Good agreement has been achieved between experiments and fully converged quantum-mechanical calculations for the $H+H_2$ reaction and the $F+H_2$ transition state.[2,3] The connection between product polarization and the reaction mechanism (and the potential-energy surface), however, is less firmly established. This lack of information is partly caused by the fact that few studies have measured product polarization with scattering-angle resolution, so that direct measures do not exist for the correlation between the product velocity and rotation (v-J correlation).

Recently, the measurement of product polarization as a function of scattering angle has been achieved from photoinitiated reactions with laser detection.[4–9] The high product density from this technique allows the state-specific laser detection of the products; such laser-based techniques are readily adaptable to the measurement of polarization parameters. Measurements of polarization-dependent differential cross sections directly provide the three-vector correlation of the reagent velocity, product velocity, and rotational polarization. Hence, the results of such experiments promise to reveal the role of product rotation in the reactive process.

This paper presents product rotational polarization studies of the gas-phase reactions of atomic chlorine with deuterated methane and ethane to give $DCl(v'=0,J'=1)$

$$Cl(^2P_{3/2})+CD_4 \rightarrow DCl(v'=0,J'=1)+CD_3, \tag{1}$$

$$Cl(^2P_{3/2})+C_2D_6 \rightarrow DCl(v'=0,J'=1)+C_2D_5. \tag{2}$$

The reaction of chlorine with deuterated methane [reaction (1)] is slightly endothermic, $\Delta H=+2.7$ kcal/mol (940 cm^{-1}, 0.118 eV), and the activation energy is estimated to be $+3.9$ kcal/mol (1370 cm^{-1}, 0.17 eV). These energies have been calculated by Simpson *et al.*[10] by correcting the analogous values for the $Cl+CH_4$ reaction[11] using the harmonic approximation. In contrast, the reaction of chlorine with deuterated ethane [reaction (2)] is nearly thermoneutral, $\Delta H=-0.25$ kcal/mol (-90 cm^{-1}, -0.01 eV)[12] and has a smaller activation energy that is estimated to be $+0.75$ kcal/mol (260 cm^{-1}, 0.033 eV).[13] These reactions have been studied previously in this laboratory and found to

give correlated state and scattering measurements.[10,14] At a collision energy of 0.18 eV, the $Cl+CD_4$ reaction was found to be back scattered, whereas at 0.25 eV, the DCl product from the $Cl+C_2D_6$ reaction was found to scatter nearly isotropically. These results were explained with the line-of-centers model and the hard-sphere scattering model.[1,10] The line-of-centers model states that the probability of reaction is constant for collisions with kinetic energy along the line of centers in excess of the reactive barrier, and the probability of reaction is zero for other collisions. The line of centers is the axis that connects the two centers of a hard-sphere collision at the point of closest approach. The collision energy used in the experiments for the $Cl+CD_4$ reaction was only slightly larger than the activation energy; therefore, according to the line-of-centers model, only low impact parameter collisions that lead to back scattering are reactive. In contrast, the collision energy used in the experiments for the $Cl+C_2D_6$ reaction was about five times more than the activation energy; in this case, according to the line-of-centers model, reactivity is largely independent of the impact parameter and, according to the hard-sphere scattering model, isotropic scattering results. Additionally, both $Cl+CD_4$ and $Cl+C_2D_6$ reactions produce rotationally cold DCl, which often is taken to indicate that the reactions proceed through linear transition states.

At first glance, the microscopic behavior of these reactions seems very similar. Thermal rate data show, however, that the Arrhenius pre-exponential factor is about seven times larger for the $Cl+C_2H_6$ reaction than for the $Cl+CH_4$ reaction.[13] In the absence of similar data, we assume that the Arrhenius pre-exponential factor for $Cl+C_2D_6$ is significantly greater than that of $Cl+CD_4$. These kinetic measurements show that the $Cl+C_2H_6$ reaction is several times more reactive than the $Cl+CH_4$ reaction, even after differences in activation energies have been taken into account. One interpretation is that the $Cl+C_2H_6$ reaction has a larger ''cone of acceptance'' than the $Cl+CH_4$ reaction, but this conclusion seems at odds with the observed cold rotational distributions, which, using an impulsive release model, would predict that both reactions should have collinear transition states. Kandel *et al.*[14] discussed this discrepancy. They proposed that the rotational distributions are manifestations of different reactive transition states. In particular, the $Cl+CH_4$ transition state was proposed to be tightly constrained and collinear, in accord with conventional wisdom, whereas the $Cl+C_2H_6$ transition state was proposed to be much less constrained. Cold rotational distributions were posited to result from a reactive mechanism in which little torque is applied to the HCl product.

The aim of this paper is to investigate directly the forces experienced by the DCl product at the transition state. This goal is achieved by measuring the alignment of the axis of rotation of the DCl product with respect to the laboratory recoil velocity and the scattering plane as a function of scattering angle. The measurements reported in this paper concern the DCl product polarization from the $Cl+CD_4$ and $Cl+C_2D_6$ reactions in which only a single quantum state, DCl ($v'=0$, $J'=1$), is probed. The reason for this choice is two fold. Both reactions yield products with cold rotational distributions that peak at or close to $J'=1$. Therefore, this product state is representative of the dynamics of these reactions. Additionally, the complete description of the polarization of the $J'=1$ product from a chemical reaction (from unaligned reagents) requires the measurement of only five parameters, the $1/\sigma(d\sigma_{00}/d\Omega_r)$, $A_1^{(1)\mathrm{stf}}$, $A_0^{(2)\mathrm{stf}}$, $A_1^{(2)\mathrm{stf}}$, and $A_2^{(2)\mathrm{stf}}$ [where the $A_q^{(k)\mathrm{stf}}$ are given by the $(d\sigma_{kq}^{\mathrm{stf}}/d\Omega_r)/(d\sigma_{00}/d\Omega_r)$[15]]. From these measurements, we hope to discern the microscopic differences that account for the differing macroscopic reactivities of the $Cl+CD_4$ and C_2D_6 reactions.

II. EXPERIMENT

The experimental apparatus and techniques have been described elsewhere, and a brief overview is detailed here.[16] Molecular chlorine (Matheson Gases, 99.999%), CD_4 or C_2D_6 (Cambridge Isotopes, 98% D-atom purity), and helium carrier gas (Liquid Carbonic, 99.995%) are coexpanded through a pulsed nozzle (General Valve 9-Series, 0.6 mm orifice) into the vacuum chamber from a backing pressure of 380 Torr. The translational cooling of the supersonic expansion ensures that the laboratory speeds of the photolytic precursor, Cl_2, and the target molecule, CD_4 or C_2D_6, are nearly the same so that their difference can be neglected. Additionally, the coexpanded molecules are assumed to be vibrationally and rotationally cold (contaminant HCl is measured to have a rotational temperature of 15 K). Monoenergetic $Cl(^2P_{3/2})$ atoms are produced by the laser photolysis of Cl_2,[17] which defines the collision energy of the Cl atoms with the target molecules. The $Cl+CD_4$ reaction is initiated by the photolysis of Cl_2 with linearly polarized 303.5 nm light (30–40 mJ/pulse), produced from the frequency-doubled output of a Nd^{3+}:YAG-pumped tunable dye laser (Continuum PL9020 and ND6000; Exciton, Rhodamine 640 dye); this photolysis wavelength gives a collision energy of 0.28 eV for the $Cl+CD_4$ reaction. The $Cl+C_2D_6$ reaction is initiated by the photolysis of Cl_2 with linearly polarized 355 nm light (90–110 mJ/pulse) from the third harmonic of the Nd^{3+}:YAG laser; this photolysis wavelength gives a collision energy of 0.25 eV for the $Cl+C_2D_6$ reaction.

Products are allowed to build up for 100 ns before the DCl ($v'=0$, $J'=1$) products are detected via $(2+1)$ REMPI through the $F\ ^1\Delta_2-X\ ^1\Sigma^+$ (0,0) $R(1)$ transition. The linearly polarized 241.1 nm probe light (1–5 mJ/pulse) is generated from the frequency-doubled output of a Nd^{3+}:YAG-pumped tunable dye laser (Spectra-Physics DCR 2A and PDL-3; Exciton, LD489 dye), and it intersects the ionization region at the focus of a 1.1 m lens. The DCl^+ is detected with a Wiley–McLaren time-of-flight mass spectrometer operated under velocity-sensitive conditions using the core-extraction method.[16] The polarization-dependent time-of-flight profiles are analyzed with the methods described in the companion paper to give the laboratory speed distribution and the speed-dependent polarization parameters. The values of the s_k in Eq. (16) of the preceding paper associated with the detection of DCl ($v'=0$, $J'=1$) via $(2+1)$ REMPI through the $F\ ^1\Delta_2-X\ ^1\Sigma^+$ (0,0) $R(1)$ transi-

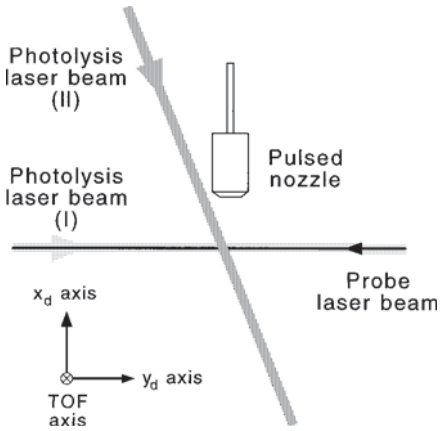

FIG. 1. Laser beam experimental geometries. The probe beam always propagates along the y_d axis. The photolysis laser beam is used in two geometries: (I) The photolysis beam counter-propagates with respect to the probe laser beam. In this position, ϵ_{phot} is employed along the x_d and z_d axes. (II) The photolysis beam propagates along the x'_d axis. In this position, ϵ_{phot} is employed along the y'_d and O' axes.

tion were calculated using the methods described by Kummel *et al.*[18] these values were calculated to be $s_1(\beta=45°)=-1$ and $s_2(\beta=0°)=1$.

We define the detection-frame coordinate system as follows: The z_d axis is parallel to the time-of-flight axis (the detection axis), and the probe laser beam propagation axis is always parallel to the y_d axis (Fig. 1). The probe polarization is flipped on a shot-to-shot basis between the z_d axis (parallel to the time-of-flight) and the x_d axis. The polarization flipping is effected by synchronization to the stress cycle of a photoelastic modulator (Hinds International, PEM-80), and the resulting polarizations have a transmittance ratio of at least 64:1 through a linear polarizer. We frequently performed *in situ* measurements to confirm that the polarization flipping did not adversely affect the laser beam power or properties in a biased manner. These measurements consisted of detecting unaligned contaminant HCl, which showed that the signal intensities varied by less than 1% between the two polarization states.

For the alignment parameter measurements, the photolysis laser beam polarization is used in three different geometries. For two of these geometries, the photolysis beam counter-propagates with respect to the probe laser and is gently focused with a 35 cm lens to a 1 mm beam at the reaction region. In this configuration, the photolysis polarization is aligned along the x_d axis or the z_d axis with a half-wave plate. Ideally, the third photolysis polarization geometry, along the y_d axis, would be obtained by propagating the photolysis laser beam along the x_d axis, but the presence of the pulsed nozzle prevents this. Consequently, the photolysis laser beam is directed in the x_d-y_d plane at 25° to the x_d axis, barely missing the pulsed nozzle (Fig. 1). The photolysis beam is focused with a 50 cm cylindrical lens and a 1 m spherical lens to a 5×0.5 mm beam; these conditions allow the probe and photolysis laser beams to overlap in the reaction region in an equivalent manner to the counter-propagating geometry. In this configuration, the third photolysis polarization geometry is perpendicular to the time-of-flight axis and parallel to the axis we define as y'_d.

TABLE I. The relative orientation of the laboratory axes described in the text, with respect to the time-of-flight axis (θ_d and φ_d are the spherical polar angles about the TOF axis). For example, in the text, the notations Z, z_d, and $\parallel$ are used to refer to axes that are parallel to the TOF axis, whereas the notations X, x_d, and $\perp$ refer to axes that are parallel to an axis that is 90° to the TOF axis with an azimuthal angle of 0°.

Notation	θ_d	φ_d
$X,x_d,\perp$	90°	0°
X',x'_d	90°	−25°
Y,y_d	90°	90°
Y',y'_d	90°	65°
$Z,z_d,\parallel$	0°	0°
O'	45°	65°
O	45°	0°

For the measurements of orientation moments, a quarter-wave plate is placed after the photoelastic modulator with its optical axis at 45° to either linear probe polarization. This wave plate thus produces right and left circularly polarized light on a shot-to-shot basis. Also, a fourth photolysis polarization geometry is used in which the photolysis polarization is 45° to the time-of-flight axis parallel to the axis we define as O' (Table I). The O' axis breaks reflection symmetry with respect to the plane defined by the probe propagation axis and the detection axis and thus allows the detection of orientation parameters. A better position for the photolysis polarization that would improve the sensitivity to the $A_1^{(1)\text{stf}}$ parameter would have been the O axis (Table I). This geometry was not realized, however, when the experiments were conducted, though this additional sensitivity did not prove to be crucial. We refer to the time-of-flight profiles from a particular geometry as I_G^F, where F refers to the geometry of the photolysis polarization and G refers to the geometry of the probe polarization. The experimental geometries described above are summarized in Table I. Henceforth, we will refer to them using the I_G^F notation.

For differential-cross-section measurements, ion-arrival profiles measured at short photolysis-probe laser delays are subtracted from long delay ion-arrival profiles on a shot-to-shot basis; only signals that grow with time survive this subtraction. This time-dependent subtraction was not used, however, for rotational anisotropy measurements. Instead, we chose to detect $D^{37}Cl^+$ to avoid the subtraction procedures necessary to separate $D^{35}Cl^+$ and nonresonantly produced $^{37}Cl^+$. The only nonreactive signal in the mass 39 region is $D^{37}Cl$ contaminant present in the beam expansion. Once the differential cross section has been measured, correcting the isotropic profiles for the $D^{37}Cl$ contaminant is simple. Even more important, this contaminant does not disrupt the measurement of rotational anisotropy, as the polarization parameters are proportional to the difference of the profiles with the probe polarization parallel and perpendicular to the time-of-flight axis and the contribution from the DCl contaminant is eliminated in this subtraction because the DCl contaminant is unaligned. As described in the next section, the polariza-

tion parameters of DCl products from chemical reactions vary with time in a fashion that makes it convenient to avoid the time-dependent subtraction procedure.

III. POLARIZATION PARAMETERS AND HYPERFINE DEPOLARIZATION

In this paper, we describe product rotational polarization at a particular laboratory velocity with the polarization parameters $A_q^{(k)}$ (where $k \leqslant 2J$ and $-k \leqslant q \leqslant k$) that are described elsewhere.[19,20] Briefly, the symmetry of the scattering plane ensures that the $A_q^{(k)}$ of k even are purely real, the $A_q^{(k)}$ of k odd are purely imaginary, the $A_0^{(k)}$ with k odd vanish, and the $A_q^{(k)}$ follow the relation[21]

$$A_q^{(k)} = (-1)^{k+q} A_{-q}^{(k)}, \tag{3}$$

where the $A_q^{(k)}$ are defined with respect to a coordinate frame whose z axis is included in the scattering plane. The $A_q^{(k)}$ as a function of scattering angle are equivalent to the $(d\sigma_{kq}/d\Omega_r)/(d\sigma_{00}/d\Omega_r)$.[15]

The time-dependent effects of hyperfine depolarization on the polarization parameters are well understood,[21–23] and we summarize the important results here. The total angular momentum for the $X\ ^1\Sigma^+$ ground electronic state of DCl, F, is the vector sum of the rotational angular momentum, J, and the nuclear angular momenta of the Cl and D nuclei, I_{Cl} and I_{D} ($I_{\mathrm{Cl}} = 3/2$ for both isotopes of chlorine, whereas $I_{\mathrm{D}} = 1$). In this experiment, the bandwidth of our probe laser is much broader than the hyperfine splitting that results from the coupling of J with the nuclear spins. Therefore, we detect individual values of J without resolving the hyperfine states. This procedure causes the observed distribution of J to be affected in a time-dependent manner by the precession of J about F, resulting in the depolarization of J with time. The measurement and quantitative description of the depolarization of HCl ($v=1$, $J=1$) has been performed in this laboratory.[24] The time-dependent factor, $G_e^{(k)}(t)$, relates the nascent polarization parameters, $A_q^{(k)}$ (J, $t=0$), to the observed polarization parameters at a time t', $A_q^{(k)}$ (J, $t=t'$), from a chemical reaction in which products build linearly with time

$$A_q^{(k)}(J, t=t') = G_c^{(k)}(t') A_q^{(k)}(J, t=0). \tag{4}$$

All experiments were conducted detecting $D^{37}Cl$ ($v=0$, $J=1$) at a time delay of 100 ns. Electric resonance measurements by Kaiser[25] show that the effect of the deuterium quadrupole moment is negligible on the 100 ns time scale ($eqQ_{\mathrm{D}} = 187$ kHz). Therefore, we make hyperfine corrections using the calculations for $D^{37}Cl$ ($v=0$, $J=1$) for which the contributions from the deuterium quadrupole have been ignored. Figure 2 illustrates $G_e^{(k)}(t)$ for $D^{37}Cl$ ($v=0$, $J=1$) and $k=1$ and 2. This figure shows that at the 100 ns time interval, the nascent values of the polarization parameters with $k=1$ and 2 are reduced to 0.45 and 0.3, respectively. Because all experiments were conducted at 100 ns delays, the measured $A_q^{(k)}$ of $k=1$ and 2 are corrected by these values.

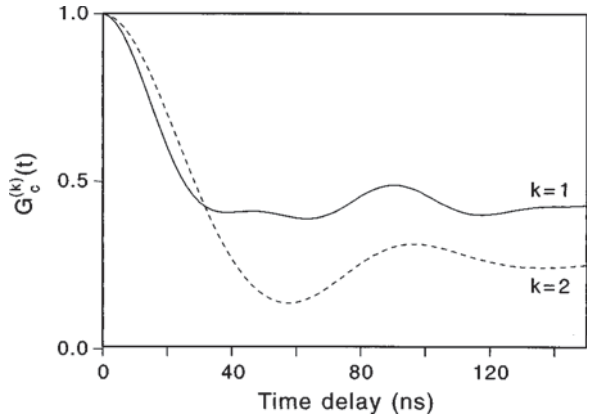

FIG. 2. The time dependence of the hyperfine depolarization factor $G_e^{(k)}(t)$ for $D^{37}Cl$ ($v=0$, $J=1$) and $k=1$ and 2. This factor shows the time dependence of the polarization parameters, $A_q^{(k)}$, of $D^{37}Cl$ ($v=0$, $J=1$) products from a chemical reaction that builds linearly with time.

IV. RESULTS

A. The Cl+CD$_4$ reaction

The kinematics of the $Cl+CD_4$ reaction constrain the laboratory scattering angle (the angle between the velocity vectors of the reagent Cl and product DCl) to be always less than 20°. As discussed in the previous paper, this constraint decreases the sensitivity to the noncylindrically symmetric moments, the $A_1^{(2)\mathrm{stf}}$ and $A_2^{(2)\mathrm{stf}}$, and thus the $A_0^{(2)\mathrm{stf}}$ parameter can be measured using two experimental geometries, $I_{\parallel}^X$ and $I_{\perp}^X$ (defined in Table I). For these geometries and for a laboratory scattering angle of 20°, Fig. 3 illustrates that the experimental sensitivity to maximal values of the $A_1^{(2)\mathrm{stf}}$ and $A_2^{(2)\mathrm{stf}}$ is several times less than the sensitivity to the $A_0^{(2)\mathrm{stf}}$ parameter, which has been chosen to be one quarter of its maximal value. Overall, under these conditions, the experimental measurement is at least 20 times more sensitive to the $A_0^{(2)\mathrm{stf}}$ parameter than to the $A_1^{(2)\mathrm{stf}}$ and $A_2^{(2)\mathrm{stf}}$ parameters. Therefore, to excellent approximation, we can attribute the product polarization-dependent signal to the $A_0^{(2)\mathrm{stf}}$ only. We define the composite profiles of experimental signals as follows:

$$I_{\mathrm{aniso}}^X = 2(I_{\parallel}^X - I_{\perp}^X) \tag{5}$$

and

$$I_{\mathrm{iso}}^X = I_{\parallel}^X + 2I_{\perp}^X. \tag{6}$$

The time-of-flight profiles, I_{aniso}^X and I_{iso}^X, of the $D^{37}Cl$ ($v'=0$, $J'=1$) product from the $^{37}Cl+CD_4$ reaction are shown in Fig. 4. The I_{iso}^X profile is polarization independent and proportional to the laboratory speed distribution only. The I_{aniso}^X profile is proportional to the laboratory speed-dependent $A_0^{(2)\mathrm{stf}}$ parameter only. These profiles are analyzed with the methods described in the previous paper. The speed distribution and differential cross section for the $D^{37}Cl$ ($v'=0$, $J'=1$) product state are shown in Fig. 5, where the scattering is shown to be predominantly in the backward hemisphere. The shape of the I_{aniso}^X profile is very interesting [Fig. 4(b)]. The core-extraction technique gives a one-to-one

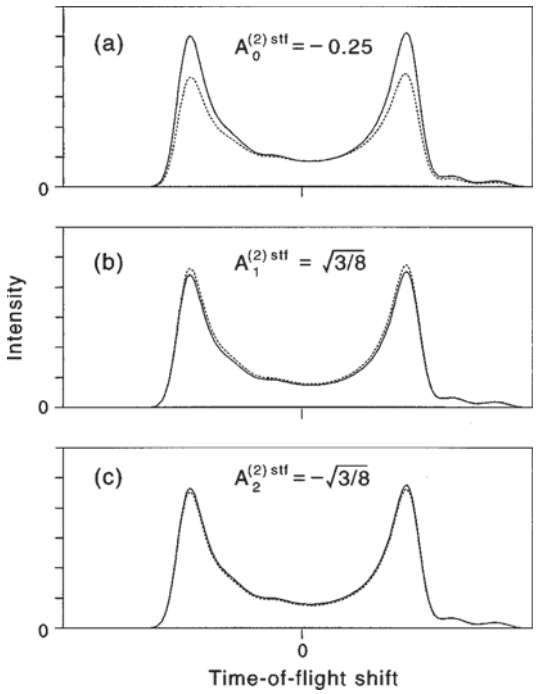

FIG. 3. Core-extracted basis functions for DCl product from the $Cl+CD_4$ reaction with a maximal laboratory scattering angle, $\theta_u = 20°$ (ignoring the effects of hyperfine depolarization). The experimental geometries are $I_{\parallel}^X$ (solid lines) and $I_{\perp}^X$ (dashed lines). (a) Basis function exhibiting $A_0^{(2)stf} = -0.25$ only; (b) $A_1^{(2)stf} = \sqrt{3/8}$ only; (c) $A_2^{(2)stf} = -\sqrt{3/8}$ only. This figure shows that, for these conditions, the experimental sensitivity to the quarter-maximal $A_0^{(2)stf}$ parameter is at least five times more than the sensitivity to maximal values of the $A_1^{(2)stf}$ and $A_2^{(2)stf}$ parameters.

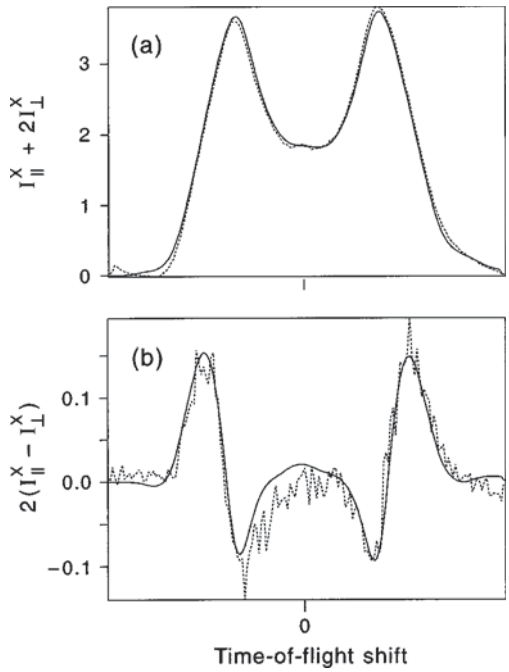

FIG. 4. (a) Core-extracted ion-arrival composite profile, I_{iso}^X, for $D^{37}Cl$ ($v' = 0$, $J' = 1$) from the $Cl+CD_4$ reaction, along with the calculated best fit function. This composite profile, $I_{iso}^X = I_{\parallel}^X + 2I_{\perp}^X$, measured with the probe polarization parallel and perpendicular to the time-of-flight axis, is independent of rotational anisotropy and is proportional to the differential cross section only. (b) Composite profile $I_{aniso}^X = 2(I_{\parallel}^X \cdot I_{\perp}^X)$ along with the calculated best fit function. This profile is proportional to the $A_0^{(2)stf}$. The solid line shows the fit to the data as a sum of instrumental basis functions obtained through a least-squares fitting algorithm. The I_{iso}^X and I_{aniso}^X profiles are plotted on the same relative vertical scale.

mapping between time-of-flight and laboratory speed (and hence scattering). Because the I_{aniso}^X profile is proportional to the $A_0^{(2)stf}$ parameter, it is clear upon inspection that this parameter is strongly negative for the back-scattered product (the slower product, in the inner part of the experimental profile) and that it inverts very suddenly to be strongly positive for the side-scattered product (the faster products, on the outer edges of the experimental profile). Because the forward-scattered intensity is very low, the $A_0^{(2)stf}$ parameter in this region is not well determined, but it seems to be tending toward a negative value again. The results of the fit of I_{aniso}^X are shown in Fig. 6, where the quantitative results confirm our expectations from Fig. 4(b). The strong dependence of the $A_0^{(2)stf}$ parameter on the scattering angle provides the key for the determination of the mechanism of rotational alignment for the $Cl+CD_4$ reaction.

B. The $Cl+C_2D_6$ reaction

For the $Cl+C_2D_6$ reaction, the kinematics do not constrain the laboratory scattering angle to be small for all scattering angles. In contrast to the $Cl+CD_4$ reaction, alignment measurements for the $Cl+C_2D_6$ reaction have significant sensitivity to the $A_1^{(2)stf}$ and $A_2^{(2)stf}$ parameters. Additionally, we measure the $A_1^{(1)stf}$ orientation parameter. Experiments using linearly polarized probe light measure the $A_0^{(2)stf}$, $A_1^{(2)stf}$, and $A_2^{(2)stf}$ parameters, whereas circularly polarized light is used to measure the $A_1^{(1)stf}$ parameter.

To measure the three $k=2$ alignment parameters, we record probe polarization difference profiles with the photolysis polarization in three different geometries, parallel to the X, Y', and Z axes (defined in Table I). Note that the Y' axis is not quite parallel to the Y axis. As before, we define

$$I_{iso}^F = I_{\parallel}^F + 2I_{\perp}^F \quad (F = X, Y', Z) \tag{7}$$

and

$$I_{aniso}^F = 2(I_{\parallel}^F - I_{\perp}^F) \quad (F = X, Y', Z). \tag{8}$$

The profiles I_{iso}^F are, to a good approximation, independent of product polarization. The summation $I_{\parallel}^F + 2I_{\perp}^F$ rigorously eliminates the $A_0^{(2)stf}$ parameter, which is responsible for the bulk of the polarization effects; the $A_1^{(2)stf}$ and $A_2^{(2)stf}$ parameters are not eliminated, but because their contribution to the total signal is less than 10%, the errors introduced to the speed distribution are small. Measurements by Kandel *et al.*[14] showed that for the $Cl+C_2H_6/C_2D_6$ reactions, the ethyl radical product receives little energy into internal modes. This finding allows us to treat these reactions as atom+diatom reactions, for which we know unambiguously the laboratory scattering angle θ_u as a function of laboratory speed, v_{DCl}^{lab}. This approximation is important because the $A_1^{(1)stf}$, $A_1^{(2)stf}$, and $A_2^{(2)stf}$ parameters depend strongly on the

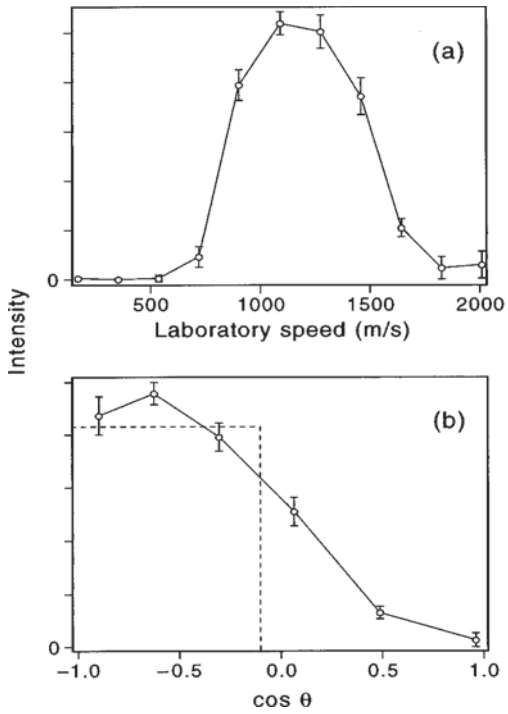

FIG. 5. (a) Speed distribution of $D^{37}Cl$ ($v'=0$, $J'=1$) from the $Cl+CD_4$ reaction resulting from a maximum-entropy analysis that fits the arrival profile to a combination of instrumental basis functions. Error bars represent 2σ statistical deviations of replicate measurements. (b) Differential cross section for the reactive product $D^{37}Cl$ ($v'=0$, $J'=1$), calculated from the measured speed distribution. The calculation assumes that internal modes of the unobserved CD_3 product are not excited. The dashed line is the prediction of the line-of-centers model with hard-sphere scattering.

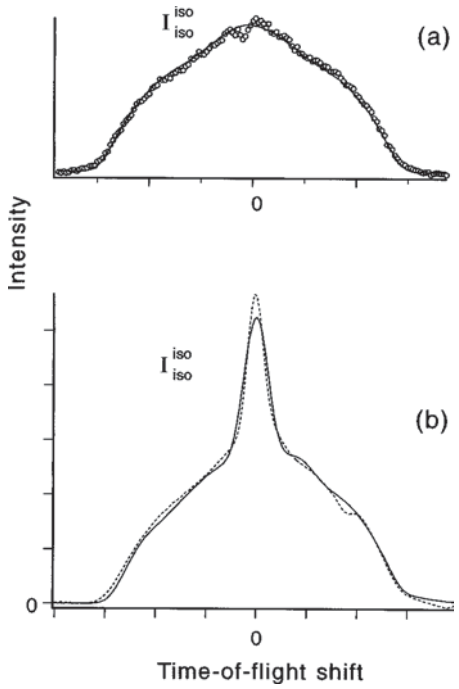

FIG. 7. (a) Core-extracted ion-arrival composite profile, I^{iso}_{iso}, for $D^{37}Cl$ ($v'=0$, $J'=1$) from the $Cl+C_2D_6$ reaction, along with the calculated best fit function. This composite profile, described in the text, is independent of spatial and rotational anisotropy and is proportional to the differential cross section only. (b) Composite profile, I^{iso}_{iso} obtained without the time-jump subtraction procedure, resulting in the presence of zero-velocity $D^{37}Cl$ ($v'=0$, $J'=1$) contaminant.

angle θ_u. The basis functions for the analysis of the time-of-flight profiles were generated assuming the ethyl radical is not internally excited.

Figure 7 shows the I^{iso}_{iso} composite profile. As described in the companion paper, the composite profile I^{iso}_{iso} is independent of spatial and rotational anisotropy. The analysis of I^{iso}_{iso} gives the laboratory speed distribution and the differential cross section (Fig. 8). The scattering is nearly isotropic, with a slight preference for forward scattering.

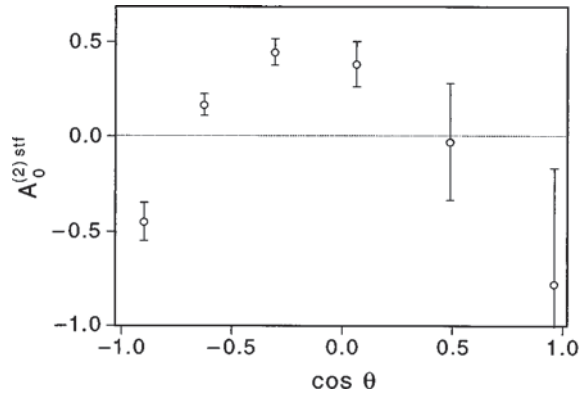

FIG. 6. Plot of the stationary target frame $(d\sigma^{stf}_{20}/d\Omega_r)/(d\sigma_{00}/d\Omega_r)$ polarization-dependent differential cross section (equivalent to the $A_0^{(2)stf}$) for the $D^{37}Cl$ ($v'=0$, $J'=1$) product from the $Cl+CD_4$ reaction, resulting from analysis of the anisotropic time profile shown in Fig. 5. Error bars represent 2σ statistical deviations of replicate measurements.

The three I^{F}_{aniso} profiles are shown in Fig. 9. These signals are proportional to the $A_0^{(2)stf}$, $A_1^{(2)stf}$, and $A_2^{(2)stf}$ parameters only. The $A_0^{(2)stf}$ parameter does not depend explicitly on the position of the photolysis polarization,[19] so the contribution of the $A_0^{(2)stf}$ is essentially the same for all three profiles. Therefore, the extent to which the three I^{F}_{aniso} profiles are different indicates the extent of the contribution from the $A_1^{(2)stf}$ and $A_2^{(2)stf}$ parameters. Figure 9 shows that the differences are substantial. The profiles are fit using the methods described in the preceding paper, and plots of the $A_0^{(2)stf}$, $A_1^{(2)stf}$, and $A_2^{(2)stf}$ versus scattering angle are shown in Fig. 10. The $A_q^{(k)stf}$ versus scattering angle are equivalent to the $(d\sigma^{stf}_{kq}/d\Omega_r)/(d\sigma_{00}/d\Omega_r)$. The error bars shown are 2σ confidence intervals, derived from the projection of the 15-dimensional 95% confidence ellipsoid (from the nonlinear least squares fit) on the $A_q^{(k)stf}$ axes. The sensitivity to the $A_0^{(2)stf}$ does not depend explicitly on the laboratory scattering angle, θ_u, whereas the sensitivity to the $A_1^{(2)stf}$ is weighted by $\sin 2\theta_u$ and the sensitivity to the $A_2^{(2)stf}$ is weighted by $\sin^2 \theta_u$. The consequence of this weighting is that the experimental sensitivity to the $A_0^{(2)stf}$ is approximately independent of the scattering angle, and the size of the error bars in Fig. 10 reflects this independence. The sensitivity to the $A_1^{(2)stf}$ parameter is poor when $\theta_u \approx 90°$ (in the back-scattered region), and the sensitivity to the $A_2^{(2)stf}$ parameter is poor

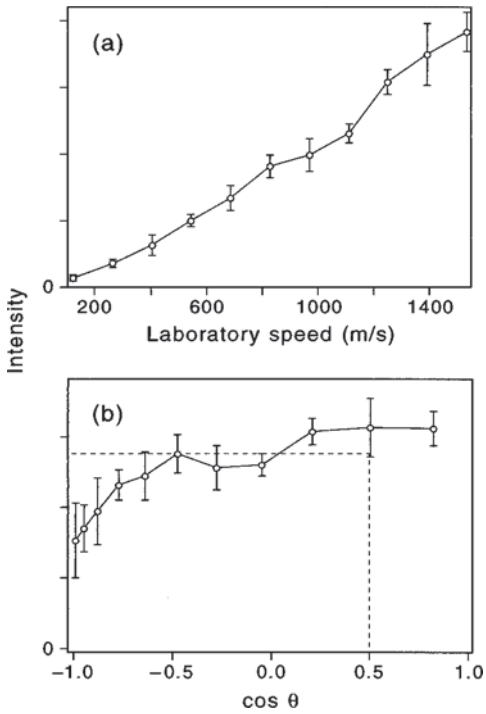

FIG. 8. (a) Speed distribution of $D^{37}Cl$ ($v'=0$, $J'=1$) from the $Cl+C_2D_6$ reaction resulting from a maximum-entropy analysis that fits the arrival profile to a combination of instrumental basis functions. The error bars are 2σ as discussed in the text. (b) Differential cross section for the reactive product $D^{37}Cl$ ($v'=0$, $J'=1$), calculated from the measured speed distribution. The calculation assumes that there is little internal energy in the unobserved C_2D_5 product, as determined by the measurements of Kandel *et al.*[14] The dashed line is the prediction of the line-of-centers model with hard-sphere scattering.

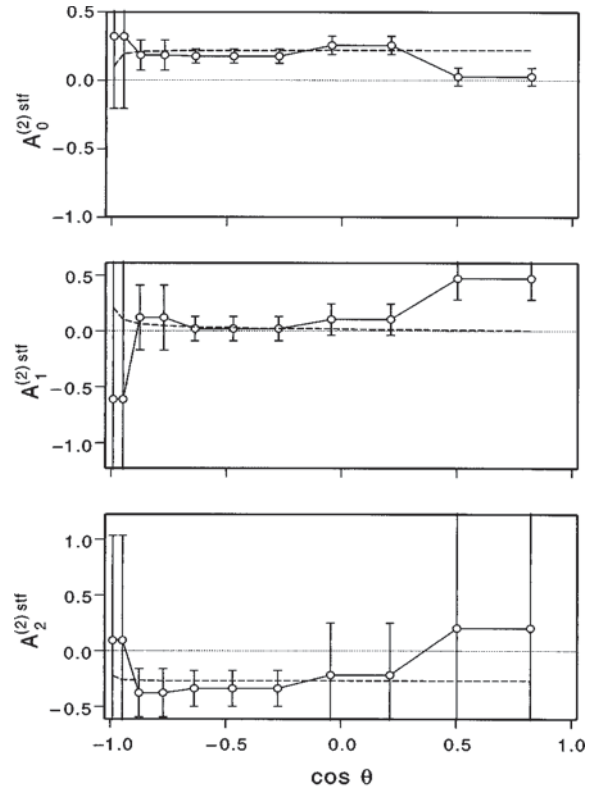

FIG. 10. Plots of the stationary target frame $A_0^{(2)\mathrm{stf}}$, $A_1^{(2)\mathrm{stf}}$, and $A_2^{(2)\mathrm{stf}}$ scattering-angle-dependent polarization parameters for the $D^{37}Cl$ ($v'=0$, $J'=1$) product from the $Cl+C_2D_6$ reaction resulting from analysis of the anisotropic time profiles shown in Fig. 9. The error bars represent 2σ confidence intervals calculated from the 15-dimensional covariance ellipsoid from the nonlinear least-squares fitting procedure. The dashed lines represent stationary target frame polarization-dependent cross sections assuming a constant product polarization in the line of centers frame, $A_0^{(2)\mathrm{loc}}=-0.5$, $A_1^{(2)\mathrm{loc}}=0$, and $A_2^{(2)\mathrm{loc}}=0$.

when $\theta_u \approx 0°$ (in the forward-scattered region); the error bars in Fig. 10 mirror these effects. Additionally, for the most back-scattered product, the laboratory speed, $v_{\mathrm{DCl}}^{\mathrm{lab}}$, is nearly equal to zero. The lack of product time-of-flight resolution for this scattering angle causes the $A_q^{(2)\mathrm{stf}}$ parameters to covary strongly, resulting in very large confidence intervals.

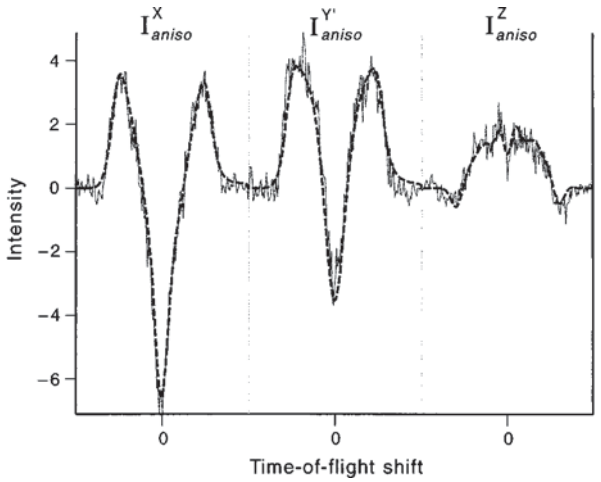

FIG. 9. The three core-extracted ion-arrival composite profiles, I^X_{aniso}, $I^{Y'}_{\mathrm{aniso}}$, and I^Z_{aniso} for $D^{37}Cl$ ($v'=0$, $J'=1$) from the $Cl+C_2D_6$ reaction along with the calculated best fit function. These profiles are proportional to the $A_0^{(2)\mathrm{stf}}$, $A_1^{(2)\mathrm{stf}}$, and $A_2^{(2)\mathrm{stf}}$ parameters. The solid line shows the simultaneous fit to all three profiles as a sum of instrumental basis functions obtained through a least-squares fitting algorithm.

To measure the $A_1^{(1)\mathrm{stf}}$ orientation parameter, we record time-of-flight profiles with right and left circularly polarized probe light and with the photolysis polarization parallel to the O' axis (defined in Table I), which breaks the reflection symmetry of the plane defined by the probe propagation direction and the detection axis (this condition is necessary to have nonzero sensitivity to the orientation parameters). We define the composite experimental profiles as follows:

$$I_{\mathrm{iso}}^{O'} = I_{+Y}^{O'} + I_{-Y}^{O'} \tag{9}$$

and

$$I_{\mathrm{aniso}}^{O'} = I_{+Y}^{O'} - I_{-Y}^{O'}. \tag{10}$$

The profile $I_{\mathrm{iso}}^{O'}$ is, to a good approximation, independent of product polarization, whereas the $I_{\mathrm{aniso}}^{O'}$ profile is proportional to the $A_1^{(1)\mathrm{stf}}$ parameter only. Figure 11(a) shows the $I_{\mathrm{iso}}^{O'}$ profile and $I_{\mathrm{aniso}}^{O'}$ profile (magnified by 10) with fits; it is clear that the $A_1^{(1)\mathrm{stf}}$ parameter is zero at all speeds within the precision of the measurement. The $(d\sigma_{11}^{\mathrm{stf}}/d\Omega_r)/(d\sigma_{00}/d\Omega_r)$

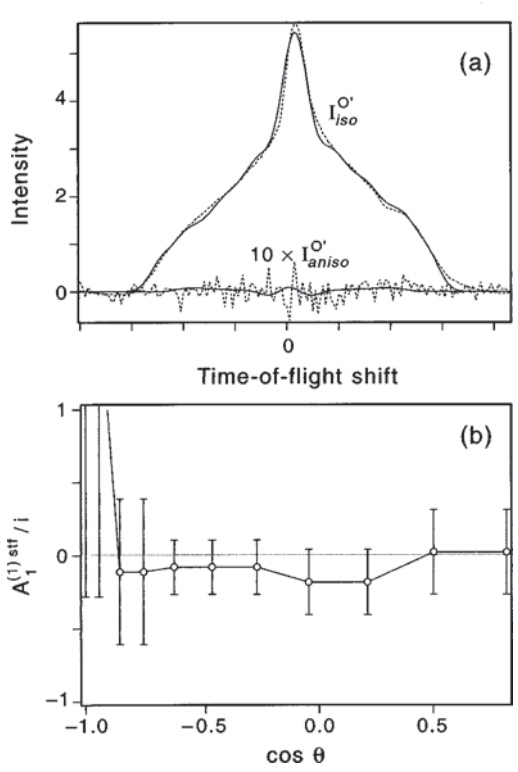

FIG. 11. (a) Core-extracted ion-arrival composite profiles $I_{\rm iso}^{O'}$ and $I_{\rm aniso}^{O'}$ for $D^{37}Cl$ ($v'=0$, $J'=1$) from the $Cl+C_2D_6$ reaction. The $I_{\rm aniso}^{O'}$ profile has been magnified by a factor of 10. (b) The $(d\sigma_{11}^{\rm stf}/d\Omega_r)/(d\sigma_{00}/d\Omega_r)$ with 2σ error bars.

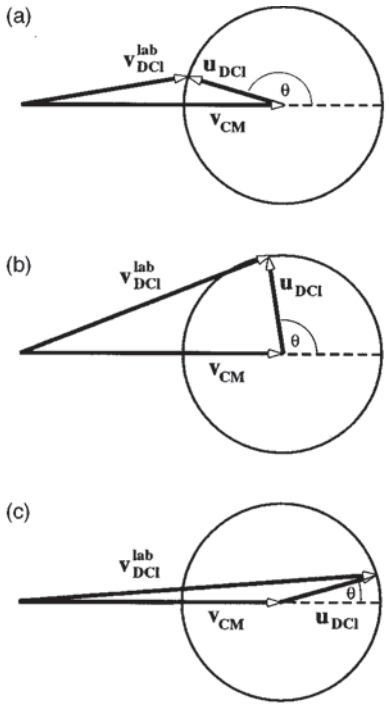

FIG. 12. Newton diagrams for the $Cl+CD_4$ reaction. (a) For the back-scattered product, $v_{\rm DCl}^{\rm lab}$ is approximately parallel to $u_{\rm DCl}$. (b) For the side-scattered product, $v_{\rm DCl}^{\rm lab}$ is approximately perpendicular to $u_{\rm DCl}$. (c) For the forward-scattered product, $v_{\rm DCl}^{\rm lab}$ is approximately parallel to $u_{\rm DCl}$.

cross section is shown in Fig. 11(b). Figures 10 and 11 may be regarded as key results for the $Cl+C_2D_6$ reaction.

V. DISCUSSION

A. $Cl+CD_4$ product alignment

The STF is unlikely to be the best reference frame for understanding reaction dynamics because the STF is defined with respect to the laboratory velocity of a particular experimental configuration. Knowledge of all three of the $A_q^{(2)\rm stf}$ parameters is necessary to calculate any $A_q^{(2)}$ parameter in another reference frame. Hence, as we have measured only the $A_0^{(2)\rm stf}$ for $Cl+CD_4$, we cannot determine directly the product alignment in an arbitrary reference frame. Instead, we elucidate the product alignment mechanism by comparing the STF parameter predictions of simple physical models to the $A_0^{(2)\rm stf}$ parameter measurements. Fortunately, the $A_0^{(2)\rm stf}$ parameter measurement versus scattering angle varies in a fashion that strongly suggests the alignment mechanism: The $A_0^{(2)\rm stf}$ parameter inverts sharply from strongly negative in the back-scattered region to strongly positive in the side-scattered region (see Fig. 6). The $A_0^{(2)\rm stf}$ parameter seems to be tending again toward negative values in the forward-scattered region, though this measurement is less certain, as there is very little forward-scattered product. One interpretation of these results would be that the alignment mechanism changes drastically with scattering angle, but we prefer another interpretation because of its simplicity. Our interpretation assumes that the alignment mechanism does not change with scattering angle, but instead, the angle between the dynamically important reference frame and the STF changes with scattering angle. In this model, the sharp STF-parameter variations are the manifestation of frame transformations. The obvious candidate for a vector that changes its angle with respect to $v_{\rm DCl}^{\rm lab}$ versus scattering angle is the product center-of-mass velocity, $u_{\rm DCl}$. Figure 12 shows that $u_{\rm DCl}$ is approximately antiparallel to $v_{\rm DCl}^{\rm lab}$ for back-scattered products, parallel to $v_{\rm DCl}^{\rm lab}$ for forward-scattered products, and approximately perpendicular to $v_{\rm DCl}^{\rm lab}$ for side-scattered products. The transformation of the polarization parameters in the product scattering frame, $A_q^{(2)\rm psf}$, to the $A_0^{(2)\rm stf}$ as a function of the angle between $v_{\rm DCl}^{\rm lab}$ and $u_{\rm DCl}$, θ_s, is given by Eqs. (11) and (12)

$$A_0^{(2)\rm stf} = \sum_{q=-2}^{2} D^2_{q0}(\varphi=0,\theta=\theta_s,\chi=0)A_q^{(2)\rm psf}, \tag{11}$$

$$A_0^{(2)\rm stf} = \tfrac{1}{2}(3\cos^2\,\theta_s - 1)A_0^{(2)\rm psf} - \sqrt{\tfrac{3}{2}}\sin 2\theta_s A_1^{(2)\rm psf} + \sqrt{\tfrac{3}{2}}\sin^2\,\theta_s A_2^{(2)\rm psf}, \tag{12}$$

where the relationship between θ_s and the scattering angle, θ, is given by

$$\tan\,\theta_s = \frac{\sin\,\theta}{\left(\dfrac{u_{\rm DCl}}{v_{\rm CM}} + \cos\,\theta\right)}. \tag{13}$$

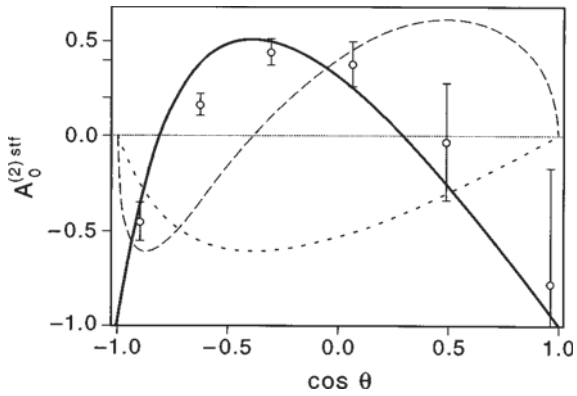

FIG. 13. Plots of the measured stationary target frame $A_0^{(2)\mathrm{stf}}$ for the $D^{37}Cl$ ($v'=0$, $J'=1$) product from the $Cl+CD_4$ reaction (data points), and the three polarization parameters with constant values in the product scattering frame, $A_0^{(2)\mathrm{psf}}=-1.0$, $A_1^{(2)\mathrm{psf}}=\sqrt{3/8}$, and $A_2^{(2)\mathrm{psf}}=-\sqrt{3/8}$.

Figure 13 shows how constant values of the $A_q^{(2)}$ in the product scattering frame transform to the $A_0^{(2)\mathrm{stf}}$. Clearly, the $A_0^{(2)\mathrm{psf}}$, with a constant and maximal value of -1.0, captures the general trend of the scattering dependence of the $A_0^{(2)\mathrm{stf}}$, in contrast, the $A_1^{(2)\mathrm{psf}}$ and $A_2^{(2)\mathrm{psf}}$ do not. Therefore, we reach the conclusion that the data can be approximated by $A_0^{(2)\mathrm{psf}}\approx-1.0$, $A_1^{(2)\mathrm{psf}}\approx0.0$, and $A_2^{(2)\mathrm{psf}}\approx0.0$. This set of scattering-angle-dependent alignment parameters implies that J_{DCl} is distributed with cylindrical symmetry in the product scattering frame and that J_{DCl} is always perpendicular to u_{DCl}.

Current work in this laboratory suggests that at low-collision energies (about 0.15 eV), most of the reactivity for $Cl+CD_4$ results from thermally populated vibrational modes of CD_4; additionally, the contribution to the reactivity from these internal modes at the collision energy studied here, 0.29 eV, may be significant (current data do not allow this statement to be quantitative). However, the kinematics of the reactions of Cl atoms with vibrationally excited CD_4 are such that constant values of $A_q^{(2)}$ in any frame cannot explain the sharp changes of the measured $A_0^{(2)\mathrm{stf}}$. Therefore, the sharp variation of the measured $A_0^{(2)\mathrm{stf}}$ can only be explained kinematically by the reaction of Cl atoms with ground-state CD_4. As before, scattering-angle-dependent polarization effects cannot be ruled out.

B. $Cl+C_2D_6$ product polarization

In contrast to the $Cl+CD_4$ reaction, we have a complete measurement of the $A_q^{(2)}$ in the STF for the DCl ($v'=0$, $J'=1$) product of the $Cl+C_2D_6$ reaction at a collision energy of 0.25 eV. Instead of making assumptions about the product alignment in other reference frames, we can transform the $A_q^{(2)\mathrm{stf}}$ directly to any other frame. As revealed in Fig. 10, with the exception of the forward-scattered region ($\cos\theta>0.5$), all three $A_q^{(2)\mathrm{stf}}$ parameters are approximately constant versus scattering angle ($A_0^{(2)\mathrm{stf}}\approx+0.2$, $A_1^{(2)\mathrm{stf}}\approx0.0$, $A_2^{(2)\mathrm{stf}}\approx-0.3$). A plot of the spatial distribution of J_{DCl} described by this measurement is shown in Fig. 14, where J_{DCl} appears to be preferentially perpendicular to an axis that is in the scattering plane but at 90° to $v_{\mathrm{DCl}}^{\mathrm{lab}}$. If we rotate the alignment parameters to this new frame described by the Euler angles ($\varphi=0$, $\theta=\pi/2$, $\chi=0$) using Eq. (14)

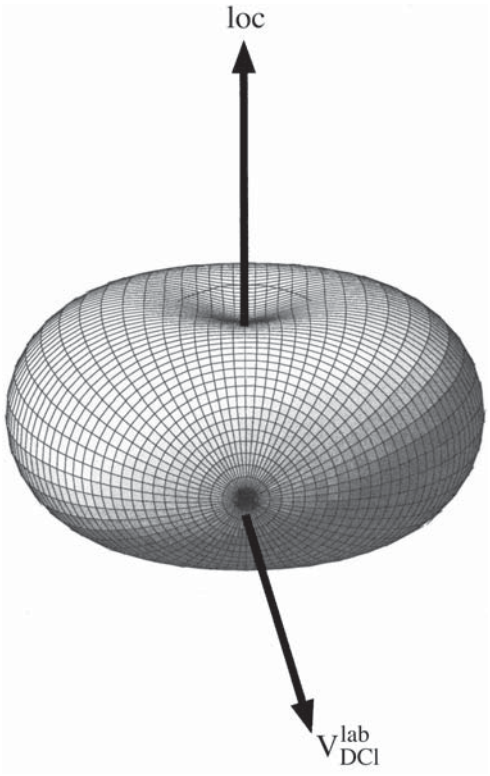

FIG. 14. The spatial distribution of J_{DCl} for DCl ($v'=0$, $J'=1$) from the $Cl+C_2D_6$ reaction constracted from the measurement, $A_0^{(2)\mathrm{stf}}\approx+0.2$, $A_1^{(2)\mathrm{stf}}\approx0.0$, and $A_2^{(2)\mathrm{stf}}\approx-0.3$. Notice that the distribution of J_{DCl} is approximately cylindically symmetric with respect to an axis that is in the scattering plane but perpendicular to $v_{\mathrm{DCl}}^{\mathrm{lab}}$.

$$A_q^{(k)\mathrm{new}}=\sum_{q'=-k}^{k}D_{q'q}^{k}(\varphi=0,\theta=\pi/2,\chi=0)A_q^{(k)\mathrm{stf}}, \qquad (14)$$

we find that the distribution of J_{DCl} is approximately cylindrically symmetric with respect to this new frame ($A_0^{(2)\mathrm{new}}\approx-0.5$, $A_1^{(2)\mathrm{new}}\approx0.0$, $A_2^{(2)\mathrm{new}}\approx0.0$). At first sight, we reach the peculiar conclusion that (except for the forward-scattered region) J_{DCl} is cylindrically symmetric to a vector in the scattering plane that is always perpendicular to the seemingly arbitrary $v_{\mathrm{DCl}}^{\mathrm{lab}}$. However, upon closer examination of a Newton diagram in which $u_{CM}=u_{AB}$, which the Newton diagram of $Cl+C_2D_6$ very closely resembles (Fig. 15), we notice that the bisector of the angle between u_{CM} and u_{AB} is rigorously perpendicular to v_{AB}^{lab}. For hard-sphere scattering, this bisector is known as the line of centers. For the $Cl+C_2D_6$ reaction, $v_{\mathrm{DCl}}^{\mathrm{lab}}$ is almost exactly perpendicular to the line of centers. Hence, the data determine that (except for the forward-scattered region) J_{DCl} is aligned in the plane perpendicular to the line of centers. The STF parameters arising from such an alignment ($A_0^{(2)\mathrm{loc}}=-0.5$, $A_1^{(2)\mathrm{loc}}=0.0$, $A_2^{(2)\mathrm{loc}}=0.0$) are shown in Fig. 10, and, of course, agree well with the data.

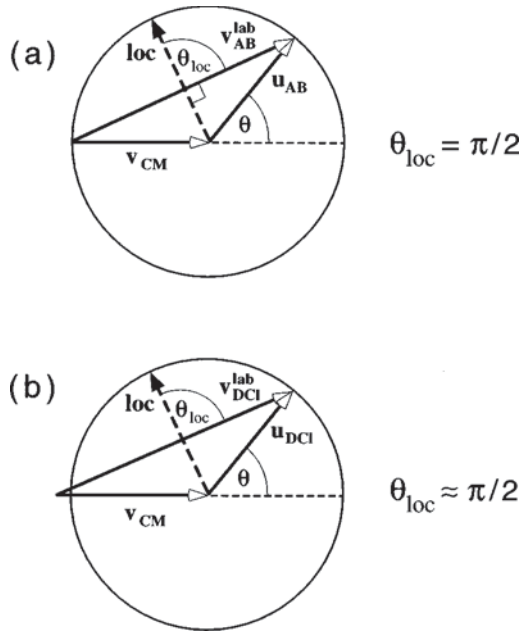

FIG. 15. (a) Newton diagram for the special case $u_{CM}=u_{AB}$, where the angle between the line of centers and $v^{\text{lab}}_{\text{DCl}}$, $\theta_{\text{loc}}=\pi/2$. (b) Newton diagram for the $Cl+C_2D_6$ reaction; the angle between the line of centers and $v^{\text{lab}}_{\text{DCl}}$, $\theta_{\text{loc}}\approx\pi/2$.

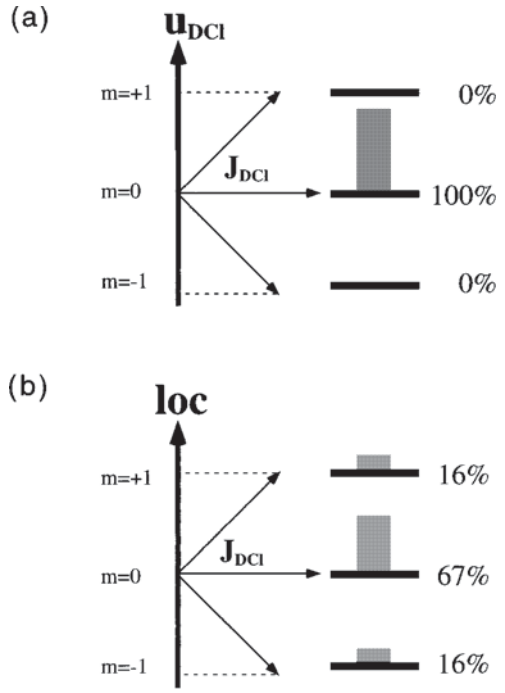

FIG. 16. M-state populations for the DCl ($v'=0$, $J'=1$) product from: (a) the $Cl+CD_4$ reaction with respect to the product separation direction, u_{DCl}; (b) the $Cl+C_2D_6$ reaction with respect to the line-of-centers direction. Notice that both reactions, in particular the $Cl+CD_4$ reaction, strongly select the $m'=0$ state. The m-state populations were calculated using Eqs. (16) and (17) and the polarization parameter measurements discussed in Secs. V A and V B.

As noted earlier, the product alignment changes suddenly in the forward-scattered region. In this region, the experimental sensitivity to the $A_2^{(2)\text{stf}}$ parameter is very poor and does not allow accurate determination of the parameter. If we assume that the alignment is cylindrically symmetric about an axis F', the values of the $A_0^{(2)\text{stf}}$ and the $A_1^{(2)\text{stf}}$ indicate that J_{DCl} is aligned perpendicularly to an axis that makes an angle of $\sim 125°$ to $v^{\text{lab}}_{\text{DCl}}$ (the counter-clockwise angle from $v^{\text{lab}}_{\text{DCl}}$ to F' is about 125°, as discussed in the next section). In particular, an alignment of $A_0^{(2)F'}\approx -1.0$, $A_1^{(2)F'}\approx 0.0$, and $A_2^{(2)F'}\approx 0.0$ gives $A_0^{(2)\text{stf}}\approx 0.0$ and $A_1^{(2)\text{stf}}\approx +0.5$, which is consistent with the data. This measurement, however, does not allow us to know unambiguously the azimuthal angle of F' about $v^{\text{lab}}_{\text{DCl}}$, which we are assuming to be 0 (placing F' in the scattering plane). Finally, the measurement of zero for the noncylindrically symmetric $A_1^{(1)\text{stf}}$ parameter is consistent with the observation from the $k=2$ parameters that J_{DCl} is distributed with cylindrical symmetry.

C. *M*-state populations

The discussion of product polarization in Sec. V A and V B used the experimentally convenient alignment parameter formalism. Using this formalism, we showed that the product polarizations for both the $Cl+CD_4$ and $Cl+C_2D_6$ reactions exhibit cylindrical symmetry about dynamically important axes and can be described with the cylindrically symmetric alignment parameters, $A_0^{(k)}$. Orr-Ewing *et al.* have reported an expression that relates the cylindrically symmetric alignment parameters to m-state populations, $p(J,m)$

$$p(J,m)=(-1)^{J-M}\sum_k \frac{(2k+1)[J(J+1)]^{k/2}}{c(k)\langle J\|J^{(k)}\|J\rangle} \times \begin{pmatrix} J & k & J \\ -M & 0 & M \end{pmatrix} A_0^{(k)}(J), \tag{15}$$

where the $c(k)$ are normalization constants[20] and the reduced matrix elements, $\langle J\|J^{(k)}\|J\rangle$, are well known.[23] Equation (15) can be evaluated to give the relationships between the m-state populations for $J=1$ and the $A_0^{(2)}$ parameter

$$p(J=1,m=0)=\tfrac{1}{3}(1-2A_0^{(2)}) \tag{16}$$

and

$$p(J=1,|m|=1)=\tfrac{1}{3}(1+A_0^{(2)}). \tag{17}$$

Equations (16) and (17) can be used to express the alignment parameter measurements from Secs. V A and V B as m-state populations (see Fig. 16). Figure 16 shows that the DCl ($v'=0$, $J'=1$) products from the $Cl+CD_4$ and $Cl+C_2D_6$ reactions exhibit a strong preference for the $m'=0$ state (albeit with respect to different z axes).

D. Rotational alignment mechanisms

Our conclusions from the previous section show that the product polarizations from the two reactions are very different yet very simple. For the $Cl+CD_4$ reaction, J_{DCl} is aligned in the plane perpendicular to the product separation direction, u_{DCl}. For the $Cl+C_2D_6$ reaction, J_{DCl} is aligned in the

plane perpendicular to the line of centers; in the forward-scattered region, the alignment of J_{DCl} is consistent with being aligned in the plane perpendicular to F', which is an axis that is intermediate between the line of centers and u_{Cl}. In this section, we present a model that can explain the observed product polarization effects.

In general, the product alignment does not allow the unambiguous elucidation of the alignment mechanism; undoubtedly, markedly different potential surfaces might give products with similar rotational polarizations. In the present case, however, we are comparing the DCl product rotational polarizations from two very similar reactions, that of chlorine atoms with deuterated methane and with deuterated ethane. Both reactions are of the kinematic type $H+LH \rightarrow HL+H$, both involve the breaking of a C–D bond and the formation of a D–Cl bond, both reactions yield rotationally and vibrationally cold products, and the scattering from both reactions can be described with the line-of-centers model. Despite these similarities, we observe that the rotational polarization from these two reactions differ significantly from each other; in addition, it is well known that $Cl+C_2D_6$ is significantly more reactive than $Cl+CD_4$. Therefore, we present a mechanism for the product alignment that aims to connect the two major dissimilarities for these two reactions.

The most obvious difference between the product alignment from the two reactions is that the alignment from the $Cl+C_2D_6$ reaction is correlated to the scattering angle, whereas the alignment from the $Cl+CD_4$ reaction is scattering-angle independent. This behavior indicates that, for the $Cl+C_2D_6$ reaction, the alignment is determined sufficiently early in the reactive process such that the reagent approach direction is dynamically significant. In contrast, for the $Cl+CD_4$ reaction, the alignment is determined late in the reactive process, at which point memory of the scattering angle has been lost.

We explain the observed product polarization effects in terms of a simple dynamical model in conjunction with the location of the D-atom transfer along the reaction coordinate. We assume that the tranfer of the D atom occurs on a time scale that is fast compared to the motion of the Cl atoms and alkyl radicals, that the transfer motion (for the ensemble average) is cylindrically symmetric with respect to the C–Cl axis at the transfer point, and that the transfer motion is responsible for the asymptotic rotational motion of the DCl. Therefore, this model predicts that the rotational axis of the DCl product will be aligned in the plane perpendicular to the C–Cl axis at the transfer point. To predict the product polarization with this model, we must know how the positions of the C and Cl nuclei vary with the reaction coordinate, and at what point the D-atom transfer occurs. As discussed at the beginning of Sec. I, we qualitatively describe the scattering behavior of the $Cl+CD_4$ and $Cl+C_2D_6$ reaction using the hard-sphere scattering model, in which the angle of incidence is equal to the angle of reflection (Fig. 17). Using this scattering model, if the D-atom transfer occurs at the point of closest approach of the C and Cl atoms, the C–Cl axis is parallel to the line of centers and thus the transfer motion is cylindrically symmetric with respect to the line-of-centers direction (Fig. 17); if the D-atom transfer occurs after the closest approach, the C–Cl axis is approximately parallel to the product separation direction, u_{DCl}, thus the transfer motion is cylindrically symmetric with respect to an axis close to u_{DCl}.

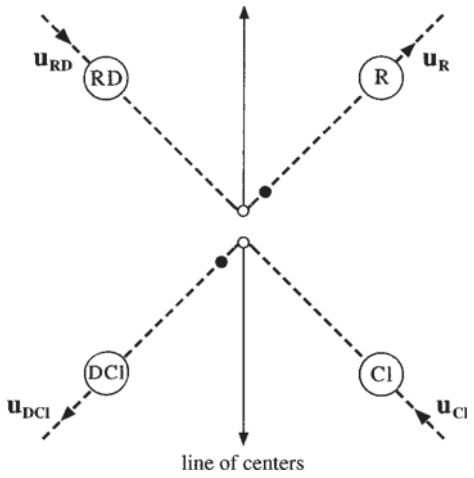

FIG. 17. Center-of-mass scattering diagram that shows that at the point of closest approach (open circles) the C–Cl axis is parallel to the line of centers, while as the products separate (black circles), the C–Cl axis is approximately parallel to u_{DCl}.

Using this model, we explain the product polarization measurements by proposing that for the $Cl+CD_4$ reaction, the D-atom transfer occurs late in the reactive process, which leads to an alignment of J_{DCl} in the plane perpendicular to an axis close to u_{DCl}. For the $Cl+C_2D_6$ reaction, we propose that the D-atom transfer occurs approximately at the point of closest approach, which leads to an alignment of J_{DCl} in the plane perpendicular to the line of centers; the sudden change in product alignment observed in the forward-scattered region is discussed later. In terms of ideas introduced by Polanyi,[26,27] the $Cl+CD_4$ reaction proceeds through a late transition state, where the tranfer point is past the closest approach of the C and Cl atoms, whereas the $Cl+C_2D_6$ reaction proceeds through an earlier transition state, where the transfer point is approximately at the closest approach of the C and Cl atoms.

It is clear from Fig. 17 that the C–Cl axis becomes closely parallel to u_{DCl} only for product separations that are large compared to the hard-sphere radii of the reactants. Therefore, according to this model, we might expect that the DCl polarization from the $Cl+CD_4$ reaction will be aligned perpendicular to an axis that is shifted from u_{DCl} toward the line of centers. In Fig. 18, we show the measured $(d\sigma_{20}^{stf}/d\Omega_r)/(d\sigma_{00}/d\Omega_r)$ for the $Cl+CD_4$ reaction along with the $(d\sigma_{20}^{stf}/d\Omega_r)/(d\sigma_{00}/d\Omega_r)$ predictions for the DCl polarization aligned in the plane perpendicular to u_{DCl}, the line of centers, and an axis that bisects u_{DCl} and the line of centers. This plot shows that the $Cl+CD_4$ rotational anisotropy data are consistent with J_{DCl} being aligned in the plane perpendicular to an axis close to u_{DCl}, whereas an alignment of J_{DCl} in the plane perpendicular to the line of centers gives

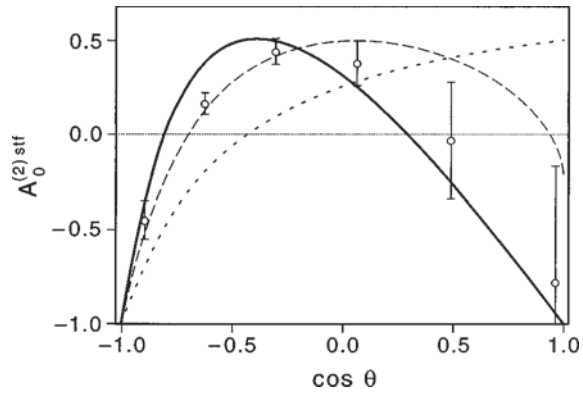

FIG. 18. Plots of the measured $A_0^{(2)\mathrm{stf}}$ parameter for the $D^{37}Cl$ ($v'=0$, $J'=1$) product from the $Cl+CD_4$ reaction and the calculated $A_0^{(2)\mathrm{stf}}$ parameter assuming a constant value for the product polarization of $A_0^{(2)}=-1.0$ with respect to an axis parallel to: u_{DCl} (solid line); the line-of-centers (dotted line); the bisector of u_{DCl} and the line of centers (dashed line). The data is consistent with a product polarization that is aligned in the plane perpendicular to an axis close to u_{DCl}.

a poor fit to the data. The important conclusion is that the DCl polarization is correlated to exit-channel vectors, and this conclusion is consistent with the model that the $Cl+CD_4$ reaction proceeds through a late transition state.

Polanyi has made predictions about the location of the reactive barrier and the effectiveness of vibrational excitation on the enhancement of reactivity.[26,27] In particular, for reactions with late barriers (in which the transition state resembles the products) reactant vibration is more efficient than translation in enhancing reactivity, whereas for reactions with early barriers (in which the transition state resembles the reactants) reactant vibration is less efficient than translation in enhancing reactivity. Previous work in this laboratory has shown that C–H stretch excitation enhances the $Cl+CH_4$ reaction by a factor of 30 at 0.16 eV collision energy,[10] whereas the $Cl+C_2H_6$ reaction is enhanced by 5% to 10% at a collision energy of 0.23 eV.[28] This dramatic difference in the effect of vibrational excitation on these two reactions is explained well using the concepts of Polanyi, where the $Cl+CH_4$ reaction is predicted to have a late barrier and the $Cl+C_2H_6$ reaction is predicted to have an earlier barrier. The qualitative conclusions about the rotational alignment are consistent with this picture. The late transition state of the $Cl+CD_4$ reaction ensures that the product rotational alignment is determined late in the reactive process, with no memory of the reagent approach direction; the earlier transition state of the $Cl+C_2D_6$ reaction allows the product rotational alignment to be determined early enough in the reactive process to show effects of the reagent approach direction.

Ab initio calculations by Truong *et al.*[29] and Duncan *et al.*[30] have shown that the $Cl+CH_4$ reaction proceeds through a late transition state. In addition, Duncan *et al.*[30] have predicted that the thermal rate of the $Cl+CH_4$ reaction is markedly enhanced by C–H stretch excitation. In contrast, the $Cl+C_2H_6$ reaction is nearly barrierless; for this reason, we expect that the atom transfer occurs approximately at the closest approach of the Cl and C atoms. We believe that the difference in the location of the atom transfer for the $Cl+CD_4$ and $Cl+C_2D_6$ reactions is responsible for the large difference in reactivity observed for these reactions (as noted in Sec. I, we expect the Arrhenius pre-exponential factor for the $Cl+C_2D_6$ reaction to be significantly larger than that of the $Cl+CD_4$ reaction). In particular, we believe that the late transition state of the $Cl+CD_4$ reaction (with a late D-atom transfer) is associated with a low probability of D-atom transfer. This behavior leads to a small Arrhenius pre-exponential factor. In contrast, the earlier transition state of the $Cl+C_2D_6$ reaction (with an earlier D-atom transfer) is associated with a high probability of D-atom transfer. This behavior leads to a larger Arrhenius pre-exponential factor. The marked enhancement in reactivity for the $Cl+CH_4$ reaction caused by C–H stretch excitation is postulated to occur as a result of to the shift of the H-atom transfer to earlier in the reactive encounter, which gives C–H stretch-excited $Cl+CH_4$ an earlier transition state, as for $Cl+C_2D_6$. Therefore, we expect that the HCl product alignment from this reaction also should change to resemble that from the $Cl+C_2D_6$ reaction. In agreement with this expectation, previous work in this laboratory showed the HCl ($v'=1$, $J'=1$) product polarization from the $Cl+CH_4$ ($\nu_3=1$) reaction to be aligned in the plane perpendicular to the line of centers.[9]

We note that the DCl ($v'=0$, $J'=1$) polarization from the $Cl+CD_4$ reaction is found to be maximally aligned ($A_0^{(2)\mathrm{psf}}\approx-1.0$), whereas that from the $Cl+C_2D_6$ reaction is found to be half-maximally aligned ($A_0^{(2)\mathrm{loc}}\approx-0.5$), albeit in different reference frames. The reduction of the degree of alignment for the DCl from the $Cl+C_2D_6$ reaction can be explained by positing that the location of the transfer of the D atoms occurs with some symmetric spread about the closest approach of the C and Cl atoms, instead of exactly at the closest approach. The averaging over the spread of transfer locations causes the reduction in the measured alignment. The symmetric spread ensures that $A_1^{(2)\mathrm{stf}}=0$, as observed. The width and functional form of the spread reduce the values of the $A_0^{(2)\mathrm{stf}}$ and $A_2^{(2)\mathrm{stf}}$; a uniform spread of $\sim 40°$ about the line of centers results in an alignment reduction that is consistent with the data. For the $Cl+CD_4$ reaction, however, the D-atom transfer occurs late in the reactive process such that small changes in the transfer location make negligible changes in the direction of the C–Cl axis, and hence there is little reduction in the product alignment in this case.

As noted earlier, in the forward-scattered region for the $Cl+C_2D_6$ reaction, the $A_0^{(2)\mathrm{stf}}$ and $A_1^{(2)\mathrm{stf}}$ parameters change suddenly (see Fig. 10). As mentioned in Sec. V A, the line-of-centers model with hard-sphere scattering breaks down and fails to predict the presence of product in the forward-scattered region. Our understanding of the polarization parameters in all but the forward-scattered region hinges on the hard-sphere scattering (specular scattering) assumption. Given that the line-of-centers model with hard-sphere scattering has broken down in the forward-scattered region, that the polarization parameters change here is not surprising. In

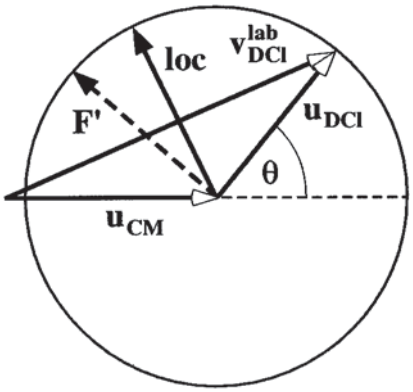

FIG. 19. The polarization of the forward-scattered DCl ($v'=0$, $J'=1$) from the $Cl+C_2D_6$ reaction is consistent with being aligned in the plane perpendicular to F', instead of the line of centers. F' is an axis that lies approximately 30° conterclockwise with respect to the line of centers.

Sec. V B, we found that in the forward-scattered region, J_{DCl} is consistent with being aligned in the plane perpendicular to the axis F' (see Fig. 19), which deviates about 30° from the line of centers. Therefore, one possible explanation for the polarization of the forward-scattered product is that it results from large-impact-parameter super-specular trajectories that have been deviated by about 30°. For a super-specular trajectory, the C–Cl axis at the point of closest approach (given here by F') is rotated counterclockwise with respect to the expected position of the line of centers if the trajectory were specular (see Fig. 19). As shown in Fig. 19, the angle between u_{CM} and F' (the angle of incidence) is smaller than the angle between F' and u_{DCl} (the angle of reflection), as is the case for super-specular trajectories.

The model for the product polarization presented here assumes that the effects of other transition-state or exit-channel forces are negligible (such as the effect of the DCl/alkyl complex on the DCl polarization). The DCl/CD_3 van der Waals complex has been shown to possess C_{3V} symmetry,[31] however, the well depth is not well known; Duncan *et al.*[30] calculated a value of 2.32 kcal/mol at the BH&HLYP level, whereas Chen *et al.* calculated a value of 0.63 kcal/mol using G1 theory.[31] The effect of the DCl/CD_3 complex on DCl product rotation is not known. If the dynamical effect of the complex is to align product rotation in the plane perpendicular to the product velocity, u_{DCl}, we note that this is not the case for the effect of the DCl/C_2D_5 complex on the DCl ($v'=0$, $J'=1$) product from the $Cl+C_2D_6$ reaction, nor the effect of the HCl/CH_3 complex on the HCl ($v'=1$, $J'=1$) product from the $Cl+CH_4$ ($\nu_3=1$) reaction.[9] (For both of these channels J_{DCl} is aligned in the plane perpendicular to the line of centers.) Without further information on the effect of the DCl/CD_3 complex on product rotation, we assume that the major forces responsible for the product alignment are transition-state forces, and not late exit-channel interactions.

VI. SUMMARY AND CONCLUSIONS

This work represents the complete description of the product polarization from the $Cl+C_2D_6 \rightarrow DCl(v'=0,J'=1)+C_2D_5$ reaction. We report the differential cross section, $1/\sigma(d\sigma_{00}/d\Omega_r)$, and all four of the stationary target frame scattering-angle-dependent polarization parameters ($A_1^{(1)stf}$, $A_0^{(2)stf}$, $A_1^{(2)stf}$, and $A_2^{(2)stf}$); additionally, we report the $1/\sigma(d\sigma_{00}/d\Omega_r)$ and the $A_0^{(2)stf}$ parameter for the $Cl+CD_4 \rightarrow DCl(v'=0,J'=1)+CD_3$ reaction. Measurements show that the product polarization from both reactions can be described in a simple fashion. For the $Cl+CD_4$ reaction, J_{DCl} is aligned in the plane perpendicular to an axis close to the product separation direction, u_{DCl}. For the $Cl+C_2D_6$ reaction (with the exception of the forward-scattered region), J_{DCl} is aligned in the plane perpendicular to the line of centers, while in the forward-scattered region, the data are consistent with an alignment of J_{DCl} in the plane perpendicular to an axis between the line of centers and u_{Cl}. We explain these results in terms of a simple model in which the rotational alignment of the DCl product is caused by the transfer motion of the D-atom, such that the DCl polarization is cylindrically symmetric with respect to the C–Cl axis at the point of transfer. We propose that the transfer point is late in the reactive process for the $Cl+CD_4$ reaction, such that the C–Cl axis is approximately parallel to u_{DCl}. For the $Cl+C_2D_6$ reaction, we propose that the transfer point is near the point of closest approach, such that the C–Cl axis is approximately parallel to the line of centers. In the context of this model, the product polarization reveals that the $Cl+CD_4$ reaction proceeds through a late transition state and the $Cl+C_2D_6$ reaction proceeds through an earlier transition state. Finally, we propose that the difference in the location of the D-atom transfer for these reactions is responsible for the differences observed in their macroscopic reactivities.

ACKNOWLEDGMENTS

S.A.K. thanks the National Science Foundation for a predoctoral fellowship. This work has been supported by the National Science Foundation under grant No. CHE-93-22690.

[1] R. D. Levine and R. B. Bernstein, *Molecular Reaction Dynamics and Chemical Reactivity* (Oxford University Press, New York, 1987).
[2] L. Schnieder, K. Seekamp-Rahn, J. Borkowski, E. Wrede, K. H. Welge, F. J. Aoiz, L. Bañares, M. J. D'Mello, V. J. Herrero, V. Sàez Ràbanos, and R. Wyatt, Science **269**, 207 (1995).
[3] D. E. Manolopoulos, K. Stark, H. J. Werner, D. W. Arnold, S. E. Bradforth, and D. M. Neumark, Science **262**, 1852 (1993).
[4] F. J. Aoiz, M. Brouard, P. A. Enriquez, and R. J. Sayos, J. Chem. Soc. Faraday Trans. **89**, 1427 (1993).
[5] M. Brouard, S. P. Duxon, P. A. Enriquez, and J. P. Simons, J. Chem. Soc. Faraday Trans. **89**, 1435 (1993).
[6] M. Brouard, S. P. Duxon, and J. P. Simons, Isr. J. Chem. **34**, 67 (1994).
[7] M. Brouard, H. M. Lambert, S. P. Rayner, and J. P. Simons, Mol. Phys. **89**, 403 (1996).
[8] H. L. Kim, M. A. Wickramaaratchi, X. Zheng, and G. E. Hall, J. Chem. Phys. **101**, 2033 (1994).
[9] A. J. Orr-Ewing, W. R. Simpson, T. P. Rakitzis, S. A. Kandel, and R. N. Zare, J. Chem. Phys. **106**, 5961 (1997).
[10] W. R. Simpson, T. P. Rakitzis, S. A. Kandel, T. Lev-On, and R. N. Zare, J. Phys. Chem. **100**, 7938 (1996).
[11] R. Atkinson, D. L. Baulch, R. A. Cox, R. F. Hampson, Jr., J. A. Kerr, and J. Troe, J. Phys. Chem. Ref. Data **21**, 1125 (1992).
[12] S. S. Parmar and S. W. Benson, J. Am. Chem. Soc. **111**, 57 (1989).

[13] E. Tschuikow-Roux, J. Niedzielski, and F. Faraji, Can. J. Chem. **63**, 1093 (1985).
[14] S. A. Kandel, T. P. Rakitzis, T. Lev-On, and R. N. Zare, J. Chem. Phys. **105**, 7550 (1996).
[15] F. J. Aoiz, M. Brouard, and P. A. Enriquez, J. Chem. Phys. **105**, 4964 (1996).
[16] W. R. Simpson, A. J. Orr-Ewing, S. A. Kandel, T. P. Rakitzis, and R. N. Zare, J. Chem. Phys. **103**, 7299 (1995).
[17] Y. Matsumi, K. Tonokura, and M. Kawasaki, J. Chem. Phys. **97**, 1065 (1992).
[18] A. C. Kummel, G. O. Sitz, and R. N. Zare, J. Chem. Phys. **88**, 6707 (1988).
[19] T. P. Rakitzis, S. A. Kandel, and R. N. Zare, J. Chem. Phys. **107**, 9382 (1997), preceding paper.
[20] A. J. Orr-Ewing and R. N. Zare, Annu. Rev. Phys. Chem. **45**, 315 (1994).
[21] K. Blum, *Density Matrix Theory and Applications* (Plenum, New York and London, 1981).
[22] U. Fano and J. H. Macek, Rev. Mod. Phys. **45**, 553 (1973).
[23] R. N. Zare, *Angular Momentum, Understanding Spatial Aspects in Chemistry and Physics* (Wiley, New York, 1988).
[24] A. J. Orr-Ewing, W. R. Simpson, T. P. Rakitzis, and R. N. Zare, Isr. J. Chem. **34**, 95 (1994).
[25] E. W. Kaiser, J. Chem. Phys. **53**, 1686 (1970).
[26] J. C. Polanyi and W. H. Wong, J. Chem. Phys. **51**, 1439 (1969).
[27] J. C. Polanyi, Acc. Chem. Res. **5**, 161 (1972).
[28] S. A. Kandel, T. P. Rakitzis, T. Lev-On, and R. N. Zare, Chem. Phys. Lett. **265**, 121 (1997).
[29] T. N. Truong, D. G. Truhlar, K. K. Baldridge, M. S. Gordon, and R. Steckler, J. Chem. Phys. **90**, 7137 (1989).
[30] W. T. Duncan and T. N. Truong, J. Chem. Phys. **22**, 9642 (1995).
[31] Y. Chen, A. Rauk, and E. T. Tschuikow-Roux, J. Phys. Chem. **95**, 9900 (1991).